

Pre-eruptive storage conditions of the Holocene dacite erupted from Kizimen Volcano, Kamchatka

Brandon Browne^{a*}, Pavel Izbekov^b, John Eichelberger^c and Tatiana Churikova^d

^aDepartment of Geological Sciences, California State University, Fullerton, CA, USA;

^bGeophysical Institute – Alaska Volcano Observatory, University of Alaska Fairbanks, Fairbanks, AK, USA; ^cUS Geological Survey Volcano Hazards Program USGS HQ – GD, 12201 Sunrise Valley Drive, Mail Stop 904, Reston, VA, USA; ^dInstitute of Volcanology and Seismology, Far East Division of Russian Academy of Sciences, Petropavlovsk-Kamchatsky, Russia

(Accepted 8 September 2009)

This study describes an investigation of the pre-eruptive conditions (T, P and fO_2) of dacite magma erupted during the KZI cycle (12,000–8400 years ago) of Kizimen Volcano, Kamchatka, the earliest, most voluminous and most explosive eruption cycle in the Kizimen record. Hydrothermal, water-saturated experiments on KZI dacite pumice coupled with titanomagnetite-ilmenite geothermometry calculations require that the KZI dacite existed at a temperature of $823 \pm 20^\circ\text{C}$ and pressures of 125–150 MPa immediately prior to eruption. This estimate corresponds to a lithologic contact between Miocene volcanoclastic rocks and Pliocene–Pleistocene volcanic rocks located at a depth of 5–6 km beneath the Kizimen edifice, which may have facilitated the accumulation of atypically large volumes of gas-rich dacite during the KZI cycle.

Keywords: Kizimen volcano; Kamchatka; magma storage; magma accumulation; experimental petrology

Introduction

Kizimen Volcano (2376 m) is a Holocene stratocone situated on the eastern edge of the Central Kamchatka Depression, where the Shchapinsky graben intersects a network of large-amplitude NE-striking normal faults (Figure 1). At least 20 tephras ranging in volume (<0.1 to $>20 \text{ km}^3$) and composition (basalt, andesite and dacite) were erupted from Kizimen Volcano during the Holocene (Melekestsev *et al.* 1995). Future large-volume eruptions seem likely, which underscores the volcanic hazard potential of the area. Despite the high frequency and compositionally heterogeneous Holocene eruptions, Kizimen Volcano is one of Kamchatka's least understood active volcanoes. Our work builds on previous stratigraphic and petrologic investigations of Kizimen Volcano by experimentally constraining the pre-eruptive storage conditions of dacite magma erupted during the KZI cycle (12,000–8400 years ago), the earliest, most voluminous and most explosive eruption cycle in the volcanic record (Melekestsev *et al.* 1995). Results from this study will serve as an important resource for future examinations of Kizimen Volcano

*Corresponding author. Email: bbrowne@fullerton.edu

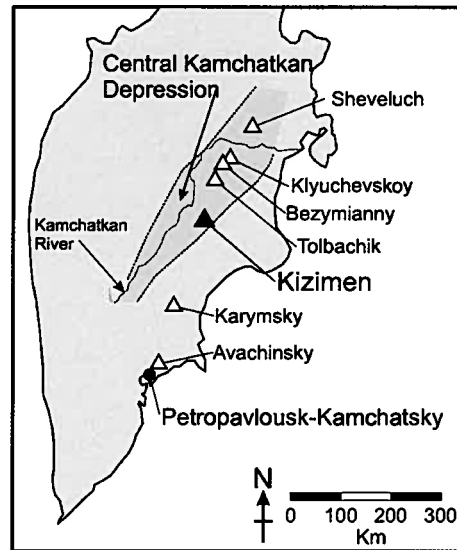


Figure 1. Simplified map of the Kamchatka Peninsula (lightly shaded) with location of Kizimen volcano (solid triangle) as well as several other historically active volcanoes (open triangles), the Central Kamchatkan Depression (dark shading), the Kamchatka River and the city of Petropavlovsk-Kamchatsky. A distance scale is also provided.

and other stratocones composed of intermediate magmas, particularly geophysical investigations designed to better understand subsurface magma plumbing systems.

Preliminary studies at Kizimen Volcano performed by Piip (1946) and Shantser *et al.* (1976) focused on the general structural characteristics of the erupted material. These studies were followed by that of Melekestsev *et al.* (1995), who combined tephrochronological and petrological techniques to divide the eruptive history into four cycles (KZI–KZIV), where each cycle was initiated by explosive activity and concluded with the effusion of a dome or lava flow. Their findings are summarized here.

The earliest Kizimen eruptive deposits were emplaced during the KZI period 12,000–8400 years ago. This phase is significant for having produced the most voluminous and explosive deposits, accounting for more than 80% of the total volume of material erupted over Kizimen's history. Moreover, magma generation rates were significantly high during the KZI cycle, estimated at $8.4 \times 10^6 \text{ m}^3/\text{year}$ compared to subsequent cycles ranging from 0.3 to $4.0 \times 10^6 \text{ m}^3/\text{year}$ (Melekestsev *et al.* 1995). KZI deposits range in whole-rock composition from silicic andesite to dacite (63–65 wt% SiO_2 ; Table 1) and are predominantly composed of distally deposited tephra and block-and-ash pyroclastic units that extend up to 15 km from the vent.

More recent eruption cycles are characterized by progressively smaller volumes and more mafic compositions (Melekestsev *et al.* 1995). Deposits from the KZII cycle (8400–6400 years ago) include a small lava dome and 1.5 – 2.0 km^3 of tephra fall deposits with glass compositions ranging from 62 to 68 wt% SiO_2 . The KZIII cycle (6400–3000 years ago) is characterized by several minor eruptions of andesitic tephra (57–63 wt% SiO_2) totaling only $\sim 0.1 \text{ km}^3$ of erupted material. During the current Kizimen eruptive cycle, KZIV (3000–present), eruptive products have been dominated by lava flows and pyroclastic units ranging from basaltic andesite to andesite (53–58 wt% SiO_2), totaling an eruptive volume of 0.7 – 1.0 km^3 . Approximately 1100 years ago an explosive lateral blast produced

Table 1. Whole-rock analyses (oxides in wt. %) of KZI dacite pumice and dome block from Melekestsev et al. (1995).

Sample	11* Pumice	12* Lava
SiO ₂	63.38	63.72
Al ₂ O ₃	15.60	16.94
TiO ₂	0.62	0.58
FeO _{tot}	5.22	4.87
MgO	0.10	0.11
MnO	2.20	1.84
CaO	5.10	5.70
Na ₂ O	3.19	3.68
K ₂ O	1.78	1.49
P ₂ O ₅	0.17	0.17
Total	97.36	99.10

FeO_{tot}, all Fe calculated as FeO.

a 1.0 × 0.7 km wide amphitheatre crater on the NE flank, followed by the effusion of a small lava dome within the newly formed crater. The only known historical eruption of Kizimen occurred from December 1928 to January 1929 and involved 'fire flames' emanating from the summit and a black eruption cloud rising from high on the NW flank where present-day fumaroles exist (Piip 1946).

Most recently, Churikova *et al.* (2001b, 2007) coupled Sr–Nd isotopic analysis of pumice and lava samples from Kizimen Volcano over the past 12,000 years with in situ minor- and trace-element zoning patterns in plagioclase crystals. One of the most important findings of the Churikova *et al.* study was that magmas erupted from Kizimen Volcano appear to have originated as a result of mixing between a cool dacite magma stored in the shallow crust and a hotter basaltic magma that intruded into the base of the dacite magma reservoir. Furthermore, Churikova *et al.* (2007) showed that mixing in the Kizimen Volcano magma reservoir does not produce a uniformly hybridized intermediate product, as evidenced by dacite lavas that contain abundant quenched basaltic enclaves and a disequilibrium mineral assemblage composed of plagioclase, hornblende, orthopyroxene, clinopyroxene and rare quartz and olivine crystals. Interestingly, some Kizimen dacite samples from the Churikova *et al.* (2007) study show no evidence of interaction with basaltic magma prior to eruption; they interpreted this to reflect mixing interrupted by the withdrawal and eruption of the incompletely blended dacite and basalt magmas shortly after intrusion of basalt into the magma chamber.

In an attempt to better understand the magma reservoir system that supplies Kizimen Volcano, our investigation experimentally constrains the pre-eruptive storage conditions of magma erupted during the earliest and most voluminous KZI cycle. A series of hydrothermal experiments performed on KZI dacite pumice provides an estimate of the pre-eruptive pressure, temperature and fO_2 conditions in the magma storage system during this eruptive period. Results show that the KZI dacite existed at a temperature of $823 \pm 20^\circ\text{C}$ and pressures of 125–150 MPa immediately prior to eruption, corresponding to a depth of 5–6 km, assuming a crustal density of 2.6 g/cm³. Interestingly, this estimate corresponds to a structural discontinuity beneath the Kizimen edifice between Miocene volcanoclastic rocks and Pliocene-Pleistocene volcanic rocks, which may have facilitated the unusually large accumulation of dacitic magma below the volcano during the earliest KZI cycle.

Materials and methods

Experimental techniques

Determining pre-eruptive storage conditions of magma ejected during a volcanic eruption involves reproducing the mineral assemblage, mineral modal abundance, and mineral textures, as well as the compositions of the minerals and coexisting melt of the natural samples, through the use of experimental petrology techniques (e.g. Rutherford *et al.* 1985; Gardner *et al.* 1995; Grove *et al.* 1997; Barclay *et al.* 1998; Hammer *et al.* 2002; Browne and Gardner 2006; Scaillet *et al.* 2008). Oxygen fugacity and temperature are first constrained by analysing Fe–Ti oxide pairs in natural samples. A series of phase equilibria experiments run at different pressures and temperatures can then be used to construct the stability fields of the most common mineral phases by plotting them in pressure-temperature space. Finally, compositions of the experimentally formed mineral rims and coexisting matrix glasses are compared with the mineral rims and coexisting matrix glass from the natural samples in order to improve the pre-eruptive storage estimate (e.g. Rutherford *et al.* 1985; Hammer *et al.* 2002).

The materials selected for phase-equilibria experiments are large portions of lightly crushed dacite pumice (01BBKZ-1) (Table 1) from a pyroclastic flow deposit located at a distance of 9 km north of Kizimen Volcano. This sample was selected because, unlike lava, pumice-forming magma ascends through the crust rapidly enough to preserve the phenocryst and melt (glass) compositions characteristic of the temperature, pressure, and fugacity of the pre-eruptive magma reservoir through quenching. In addition, neither banding nor clots of mafic material were observed in this pumice, which have been suggested by Churikova *et al.* (2007) to form through the mixing of a basaltic and dacitic magma.

All phase equilibria experiments were conducted in the University of Alaska Fairbanks Experimental Petrology Facility and performed within Ag₇₀Pd₃₀ tubing. With one end of the tubing crimped and welded, 0.1–0.5 g of powdered dacite sample (01BBKZ-1) was combined with sufficient distilled water to ensure that all samples were water-saturated ($P_{\text{H}_2\text{O}} = P_{\text{total}}$). No additional volatiles (e.g. CO₂, S) were added to the experiments. The open end of the tubing was then crimped and the capsule weight was recorded. After welding the crimped end, the capsule was heated for 1 h on a 150°C hot plate to determine whether any distilled water escaped during welding. Finally, capsules were re-weighed, and discarded if water loss occurred.

Experiments were performed in Rene cold-seal pressure vessels in which water is utilized as the pressurizing fluid. Oxygen fugacity was buffered to the Ni–NiO (NNO) oxygen buffer curve as a result of reactions between the Ni-alloy Rene pressure vessel, a Ni filler rod inserted into the vessel, and pressurized water (Geschwind and Rutherford 1992). Temperature and pressure settings in the University of Alaska Fairbanks Experimental Petrology Laboratory are precise to $\pm 3^\circ\text{C}$ and ± 0.5 MPa, respectively (Larsen and Gardner 2000). All phase equilibria experiments were held at constant pressure and temperature for 4–6 days in order to grow crystals large enough to identify and analyse. At the end of an experimental run, Rene pressure vessels were removed from their horizontal furnaces at high pressure (i.e. the pressure of a given experiment) and immediately quenched by submerging them in water at room temperature. Reversal experiments were run for most conditions.

Electron microprobe techniques

Samples were mounted in epoxy on thin sections and polished by hand. Back-scattered electron (BSE) images, as well as mineral and glass compositional analyses, were

obtained from polished thin sections of all natural and experimental samples using a JEOL JXA-8200 Superprobe, located at UCLA, and a Cameca SX-50 electron microprobe, located at the University of Alaska, Fairbanks. BSE imaging was conducted using a 2 μm -wide focused beam, an accelerating voltage of 15 KeV and a beam current ranging from 25 to 50 nA. Mineral analyses were performed through a procedure involving a 1 μm -wide focused beam at an accelerating voltage of 15 KeV, and a beam current of 10 nA. Glass analyses were acquired with a defocused electron beam ($\sim 10\text{-}\mu\text{m}$ -wide), an accelerating voltage of 15 KeV, and a beam current of 8 nA in order to minimize sodium migration. During all glass analyses, sodium concentration was monitored in 2-second intervals. Upon completion of the analysis, sodium X-ray counts, which were detected by the electron microprobe spectrometer, were regressed to determine the initial sodium content of the glass (Devine *et al.* 1995). Standards of hydrated glasses with known dissolved water contents were used prior to and following analyses of experimental samples to ensure validity of data. Mineral phases in the experiments were also identified and evaluated through the use of a traditional petrographic microscope, where phase stability was determined based on the presence of new, euhedral crystals that grew during the experiment.

Results

KZI dacite

The KZI dacite pumice sample used in this study is crystal-rich, averaging 40% crystals by volume; plagioclase and hornblende are the most common phenocryst phases with lesser orthopyroxene, magnetite, and ilmenite. Plagioclase phenocrysts are typically large, ranging from 0.3 to 0.8 mm in diameter, and are usually euhedral. Hornblende phenocrysts are also typically euhedral and elongate, ranging from 0.1 to 0.5 mm in diameter at their widest point. Although neither olivine, quartz nor clinopyroxene were observed in the KZI pumice sample used for these experiments, Melekestsev *et al.* (1995) and Churikova *et al.* (2007) report observing olivine, clinopyroxene, and quartz in trace amounts (<0.5 vol%) in some KZI dacite samples, noting that, when present, olivine is invariably rimmed by orthopyroxene and clinopyroxene is typically mantled by orthopyroxene and Fe–Ti oxides. Where quartz crystals are observed, they invariably display embayed crystal faces (Churikova *et al.* 2007).

Fe–Ti oxide geothermometry

Average compositions of coexisting titanomagnetite and ilmenite phenocrysts from the KZI dacite pumice and temperatures based on the Anderson and Lindsley (1988) geothermometer are listed in Table 2. The method of Stormer (1983) was employed to calculate the distribution of iron between Fe^{2+} and Fe^{3+} as well as mole fractions of ulvospinel and ilmenite. Titanomagnetite is abundant in KZI dacite pumice, accounting for 1–2 vol%, present as 0.03–0.6 mm, euhedral to subhedral phenocrysts and as plagioclase- and hornblende-hosted inclusions. Titanomagnetite core compositions are more variable compared to rim compositions: cores range from 4.4 to 6.6 wt% TiO_2 (12.8–18.6 mole% ulvospinel) and rims range from 4.6 to 4.9 wt% TiO_2 (12.9–14.2 mole% ulvospinel). Ilmenite is much less abundant than titanomagnetite, accounting for less than 0.5 vol% of the KZI pumice. Ilmenite forms as 0.02–0.08 mm, euhedral to subhedral grains that are either attached to titanomagnetite phenocrysts or forms as inclusions in pyroxene. Similar to titanomagnetite, ilmenite core compositions are more heterogeneous compared to

Table 2. Representative electron microprobe analyses (oxides in weight %) of touching Fe-Ti oxide cores (c) and rims (r) from KZI dacite. Iron recalculation based on the method of Stormer (1983) and calculated temperatures and oxygen fugacities for mineral pairs based on the method of Anderson and Lindsley (1988). n , number of analyses averaged; X_{Ulv} , mole fraction ulvospinel; U_{Ilm} , mole fraction ilmenite.

Sample Mineral	KZI-Mag01c core Mag	KZI-Ilm01c core Ilm	KZI-Mag02c core Mag	KZI-Ilm02c core Ilm	KZI-Mag05c core Mag	KZI-Ilm05c core Ilm	KZI-Mag06c core Mag	KZI-Ilm06c core Ilm	KZI-Mag09c core Mag	KZI-Ilm09c core Ilm
TiO ₂	4.48	28.57	4.41	28.74	4.48	28.92	4.49	29.11	6.62	36.79
Al ₂ O ₃	2.09	0.39	2.07	0.38	2.03	0.35	2.05	0.38	2.02	0.28
FeO	86.93	65.78	86.95	65.67	84.16	65.98	86.30	66.01	83.97	57.37
MnO	0.43	0.22	0.43	0.22	0.46	0.23	0.44	0.21	0.88	0.56
MgO	1.11	1.00	1.14	1.03	1.40	1.06	1.13	1.01	1.63	1.88
Cr ₂ O ₃	0.2	0.1	0.2	0.1	0.1	0.1	0.2	0.1	0.0	0.0
sum	95.2	96.0	95.2	96.1	92.6	96.6	94.6	96.8	95.1	96.9
Fe ₂ O ₃	59.1	46.8	59.2	46.5	57.5	46.8	58.6	46.4	55.1	31.3
FeO	33.8	23.7	33.7	23.8	32.4	23.9	33.5	23.3	34.4	29.2
Total	101.2	100.8	101.1	100.8	98.3	101.3	100.4	100.5	100.7	100.0
n	5	5	5	6	5	5	4	5	6	6
X_{Ulv}	13.03		12.80		15.11		13.11		18.61	
X_{Ilm}		53.98		54.22		54.23		53.76		68.79
T(°C)		858		855		875		859		855
log f_{O_2}		-10.67		-10.72		-10.47		-10.64		-11.24

Sample Mineral	KZI-Mag01r rim Mag	KZI-Ilm01r rim Ilm	KZI-Mag02r rim Mag	KZI-Ilm02r rim Ilm	KZI-Mag05r rim Mag	KZI-Ilm05r rim Ilm	KZI-Mag06r rim Mag	KZI-Ilm06r rim Ilm	KZI-Mag09r rim Mag	KZI-Ilm09r rim Ilm
TiO ₂	4.62	36.79	4.61	34.13	4.98	38.49	4.49	35.98	4.97	36.56
Al ₂ O ₃	2.02	0.28	1.97	0.34	1.46	0.51	2.14	0.65	2.16	0.76
FeO	84.67	57.37	84.94	59.18	86.35	56.37	85.97	58.21	83.46	57.13
MnO	0.88	0.56	0.79	0.62	0.43	0.29	0.44	0.21	0.87	0.55
MgO	1.63	1.88	1.64	1.85	1.11	1.03	1.12	1.02	1.98	1.64
Cr ₂ O ₃	0.02	0.00	0.00	0.00	0.10	0.02	0.40	0.00	0.00	0.00
sum	93.84	96.88	93.95	96.12	94.43	96.71	94.56	96.07	93.44	96.64
Fe ₂ O ₃	58.3	31.1	58.5	36.0	58.3	26.5	58.3	31.0	57.4	30.8
FeO	32.2	29.2	32.3	26.8	33.9	32.5	33.5	30.3	31.9	29.4
Total	99.7	99.8	99.8	99.7	100.3	99.3	100.4	99.2	99.3	99.7
X _{iliv}	13.00		12.94		14.20		13.26		13.88	
X _{ilm}		68.96		63.89		73.75		69.21		69.17
n	5	6	6	5	5	5	5	5	4	5
T(°C)		819		828		816		820		824
log fO ₂		-11.66		-11.95		-11.90		-11.65		-11.60

ilmenite rims. Whereas ilmenite core compositions range from 57.4 to 66.0 wt% FeO (53.8–68.8 mole% ilmenite), rim compositions range from 56.4 to 59.2 wt% FeO (63.9–73.8 mole% ilmenite).

Geothermometry estimates are based solely on analyses of touching titanomagnetite and ilmenite grains exhibiting euhedral or subhedral crystal faces and pair compositions characterized by Mg/Mn equilibrium partitioning as defined by Bacon and Hirschmann (1988). Typical errors for temperature and oxygen fugacity calculations are $\pm 20^\circ\text{C}$ and ± 0.15 log units, respectively. Titanomagnetite-ilmenite pairs are normally zoned, with core temperatures ranging from 855 to 875°C (average = 860°C) and oxygen fugacities ranging from $10^{-10.4}$ to $10^{-11.2}$ bars; temperatures and oxygen fugacities calculated from rim compositions vary from 816 to 828°C (average = 823°C), and $10^{-11.6}$ to $10^{-11.9}$ bars, respectively.

Phase equilibria and compositions

Twenty phase equilibria experiments were performed in order to constrain the stability fields of hornblende, plagioclase, orthopyroxene, and Fe-Ti oxides (Figure 2) in water-saturated KZI dacite (Table 3). Significant observations include the following: titanomagnetite and ilmenite are stable at all experimental conditions; plagioclase is stable at temperatures below 880°C and becomes more calcic with decreasing pressure; pyroxene is stable below 900°C; below 860°C, hornblende is stable at pressures as low as 100 MPa, but with increasing temperature, hornblende stability is restricted to higher pressures. These results are similar to many other recent experimental studies on intermediate composition magmas, including the 1989–1990 dacite eruption of Redoubt volcano, Alaska (Browne and Gardner 2006), the 1991–1995 dacite from Unzen volcano, Japan (Sato *et al.* 1999) and the 1997 andesite from Soufriere Hills volcano, Montserrat (Barclay *et al.* 1998).

The compositions of coexisting experimental phenocryst rims and matrix glasses can be used to refine equilibrium conditions based on phase assemblage (Table 4). Average

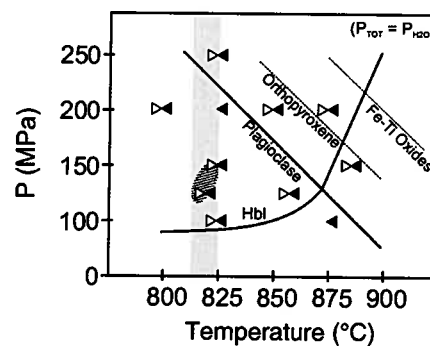


Figure 2. Phase equilibria diagram for KZI dacite (01BBKZ-1) experiments. Left- and right-pointing triangles are crystallization and melting experiments, respectively. Solid and dashed lines are 'mineral-in' curves for plagioclase, orthopyroxene, Fe-Ti oxides, and hornblende. Shaded region represents range of pre-eruptive temperatures based on Fe-Ti oxide geothermometry. Patterned region is estimated pre-eruption storage conditions where KZI dacite was stable immediately prior to eruption, based on geothermometry, phase stability, and compositions of coexisting glass and mineral phases.

Table 3. KZI dacite phase equilibria experiments.

Experiment	SM*	P (MPa)	T (°C)	Duration (days)	Products "
KZI-1	D	150	825	4.0	Pl, Hbl, Opx, Ox, gl
KZI-2	D	150	825	4.2	Pl, Hbl, Opx, Ox, gl
KZI-3	KZI-2	150	880	5.1	Opx, Ox, gl
KZI-4	KZI-2	150	880	4.8	Opx, Ox, gl
KZI-5	D	100	825	5.0	Pl, Hbl, Opx, Ox, gl
KZI-6	D	100	825	4.8	Pl, Hbl, Opx, Ox, gl
KZI-7	D	100	875	4.1	Pl, Opx, Ox, gl
KZI-8	D	200	800	5.8	Pl, Hbl, Opx, Ox, gl
KZI-9	D	200	800	5.8	Pl, Hbl, Opx, Ox, gl
KZI-10	D	200	825	4.2	Pl, Hbl, Opx, Ox, gl
KZI-11	D	200	850	4.0	Hbl, Opx, Ox, gl
KZI-12	KZI-9	200	850	4.1	Hbl, Opx, Ox, gl
KZI-13	D	200	875	4.0	Hbl, Opx, Ox, gl
KZI-14	D	200	875	4.0	Hbl, Opx, Ox, gl
KZI-15	KZI-9	250	825	4.6	Hbl, Opx, Ox, gl
KZI-16	D	250	825	4.5	Hbl, Opx, Ox, gl
KZI-17	KZI-16	125	815	5.7	Pl, Hbl, Opx, Ox, gl
KZI-18	KZI-16	125	815	5.9	Pl, Hbl, Opx, Ox, gl
KZI-19	KZI-14	125	860	5.1	Pl, Hbl, Opx, Ox, gl
KZI-20	KZI-14	125	860	4.8	Pl, Hbl, Opx, Ox, gl

*SM, Starting Material; D, crushed KZI dacite pumice 01BBKZ-1; Experiment number, products of previous experiments used as SM.

"Pl, plagioclase; Hbl, hornblende; Opx, orthopyroxene; Px, orthopyroxene; Ox, Fe-Ti Oxide; gl, glass.

rim compositions of plagioclase phenocrysts from the KZI dacite and phase equilibria experiments are listed in Table 4. Rim compositions of KZI dacite plagioclase range from An₄₉ to An₅₂. Compositions of plagioclase microlite rims grown in experiments range from An₄₆ to An₆₃ and become progressively more sodic as temperature and pressure decreased (Figure 3). Plagioclase rim compositions from experiments run at temperatures of 815°C and a pressure of 125 MPa are nearly identical to natural plagioclase rim compositions, ranging from An₄₈ to An₅₁ (Figure 3).

The composition of residual melt (i.e. glass composition) in experiment samples also varies systematically in composition with pressure and temperature (Table 5). At constant pressure, the concentration of SiO₂ and K₂O decrease with increasing temperature, whereas concentrations of Al₂O₃, MgO, and CaO increase (Figure 4). In contrast, at constant temperature, concentrations of SiO₂ and K₂O decrease with increasing pressure, whereas concentrations of Al₂O₃, MgO, and CaO increase. Finally, although the concentration of Na₂O in melt depends strongly on temperature, a systematic variation with pressure is not observed. Glass compositions from experiments run at 815–825°C and 125–150 MPa are most similar to natural glass compositions (Figure 4).

Discussion

In a water-saturated magma like that of the KZI dacite erupted from Kizimen Volcano, equilibrium compositions of mineral phases and the coexisting melt phase will be dictated by the temperature, pressure, and oxygen fugacity of the system. Magnetite-ilmenite geothermometry calculations and the experimentally derived mineral and melt phases indicate that the dacite mineral assemblage crystallized at temperatures of 825°C ± 20°C (Figure 2).

Table 4. Electron microprobe (oxides in wt.%) analyses of plagioclase rims from natural sample (01BBKZ-1) and phase equilibria experiments.

Sample	01BBKZ-1	KZI-1 ^m	KZI-2 ^c	KZI-5 ^m	KZI-6 ^c	KZI-7 ^c	KZI-8 ^c	KZI-9 ^m	KZI-10 ^c	KZI-17 ^m	KZI-18 ^c	KZI-19 ^c	KZI-20 ^c
T(°C)	(Natural)	825	825	825	825	875	825	800	800	860	860	815	815
Pressure (MPa)	Sample)	150	150	100	100	100	200	200	200	125	125	125	125
SiO ₂	59.82	54.60	54.84	55.17	55.60	55.21	52.19	53.29	53.56	54.99	55.18	59.60	56.31
Al ₂ O ₃	27.13	28.61	28.11	27.19	27.30	28.34	29.64	30.04	28.93	27.49	28.82	25.50	27.26
FeO _{tot}	0.18	0.33	0.15	0.12	0.19	0.14	0.30	0.46	0.11	0.61	0.15	0.24	0.24
CaO	8.44	10.95	10.73	10.65	9.66	11.54	11.97	12.27	13.13	10.79	10.79	9.20	9.78
Na ₂ O	4.22	5.18	5.06	6.47	6.08	4.98	4.14	4.20	4.72	4.70	4.96	4.94	5.61
K ₂ O	0.22	0.20	0.32	0.47	0.45	0.28	0.10	0.05	0.23	0.33	0.32	0.39	0.41
Total	100.01	99.87	99.21	100.07	99.28	100.49	98.34	100.31	100.68	98.91	100.22	99.87	99.61
n	14	15	12	14	13	15	16	14	13	15	15	12	13
An	50.7	53.2	52.9	46.7	45.5	55.3	61.5	63.4	59.8	55.8	53.5	49.5	48.8

n, number of analyses averaged; An, mole % Anorthite; ^m, melting experiments; ^c, crystallization experiments.

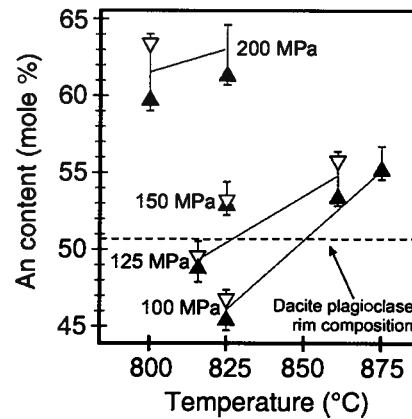


Figure 3. Plagioclase rim compositions from natural KZI dacite (dashed line) and hydrothermal experiments where plagioclase was found to be stable for different pressures and temperatures. Solid lines connect experiments conducted at equal pressures. Melting and crystallization experiments (open and solid triangles, respectively) used both pre-run aliquots and 01BBKZ-1 crushed KZI dacite pumice (Table 3).

The pre-eruptive pressure can be constrained by comparing the compositions of plagioclase rims and coexisting matrix glass in natural samples with those formed during experimental runs performed at many different pressures (e.g. Rutherford *et al.* 1985; Gardner *et al.* 1995; Izbekov *et al.* 2004; Browne and Gardner 2006). In the case of plagioclase, compositions from experimentally grown microlites are nearly identical to natural plagioclase rim compositions from runs at 125 MPa and 815°C (Figure 3). Similarly, the compositions of matrix glass from experiments closely match the composition of natural dacite matrix glass from runs at pressures of 125–150 MPa and temperatures of 815–825°C (Figure 4). The pre-eruptive temperature and pressure conditions of the KZI dacite is therefore constrained at $825 \pm 20^\circ\text{C}$ and 125 ± 25 MPa, which is consistent with a depth of 5–6 km assuming a density of 2.6 g/cm^3 for the upper crustal volcanic rocks.

A critical responsibility of experimental petrology research papers is to acknowledge potential sources of error in the findings described here so as to maximize the applicability and usefulness of the results. Beyond the errors associated with experimental and analytical precision, which are minor and clearly stated in the Methods and Materials section, perhaps the most important source of error facing this study relates to the fact that H_2O is the only volatile species used in the phase stability experiments. Other volatile species such as CO_2 , S, Cl, and F are common in dacitic magmas, although in significantly lower concentrations than H_2O (e.g. Carroll and Webster 1994; Rutherford and Devine 1996; Scaillet and Evans 1999; Churikova *et al.* 2001a, Scaillet and Pichavant 2003; Wallace 2005). Even so, results from experimental phase equilibria studies that utilize mixtures of volatile species show that the inclusion of even minor concentrations (e.g. 0.1 wt%) of other volatiles influence the abundance and composition of crystallized mineral phases. For example, Costa *et al.* (2004) conducted a series of H_2O -saturated phase equilibria experiments and a series of $\text{H}_2\text{O}+\text{S}$ -saturated phase equilibria experiments on the same dacite starting material from Volcán San Pedro (Chile). In this study, only the $\text{H}_2\text{O} + \text{S}$ -bearing experiments produced the complete phase assemblage as observed in the natural sample, including plagioclase, hornblende, orthopyroxene, magnetite, ilmenite, biotite and pyrrhotite,

Table 5. Ejection microprobe (oxides in wt%) glass analyses of natural sample (01BBKZ-1) and phase equilibria experiments.

Sample T (°C) Pressure (MPa)	KZI-1 ^m		KZI-2 ^c		KZI-3 ^m		KZI-4 ^c		KZI-5 ^m		KZI-6 ^c		KZI-7 ^c		KZI-8 ^c		KZI-9 ^m		KZI-10 ^c	
	825 150	150	825 150	880 150	880 150	880 150	880 150	880 150	825 100	825 100	825 100	825 100	875 100	875 100	800 200	800 200	800 200	800 200	825 200	825 200
SiO ₂	76.18 (0.71)	72.61 (0.64)	72.01 (0.68)	69.82 (0.72)	69.62 (0.74)	74.86 (0.91)	74.38 (1.08)	70.61 (1.02)	69.16 (0.61)	71.55 (0.77)	71.98 (0.63)									
Al ₂ O ₃	12.81 (0.13)	12.94 (0.12)	13.16 (0.15)	15.45 (0.19)	15.91 (0.17)	11.61 (0.52)	11.86 (0.64)	14.86 (0.81)	14.36 (0.19)	14.2 (0.14)	13.42 (0.19)									
TiO ₂	0.25 (0.11)	0.24 (0.09)	0.22 (0.11)	0.29 (0.12)	0.34 (0.04)	0.38 (0.11)	0.31 (0.08)	0.22 (0.04)	0.21 (0.08)	0.26 (0.04)	0.22 (0.08)									
FeO _{tot}	1.22 (0.43)	1.25 (0.38)	1.26 (0.24)	1.38 (0.31)	1.44 (0.30)	1.16 (0.16)	1.19 (0.20)	1.91 (0.08)	1.39 (0.27)	1.26 (0.11)	1.31 (0.32)									
MgO	0.22 (0.12)	0.11 (0.06)	0.13 (0.08)	0.22 (0.04)	0.29 (0.08)	0.11 (0.05)	0.13 (0.04)	0.19 (0.02)	0.2 (0.050)	0.16 (0.06)	0.11 (0.04)									
CaO	1.34 (0.11)	0.92 (0.11)	0.96 (0.09)	0.98 (0.13)	1.03 (0.18)	0.71 (0.15)	0.74 (0.12)	0.79 (0.21)	1.11 (0.08)	0.95 (0.12)	1.06 (0.08)									
Na ₂ O	3.38 (0.26)	3.02 (0.14)	3.11 (0.12)	3.33 (0.18)	3.16 (0.21)	3.33 (0.37)	3.41 (0.28)	3.62 (0.46)	2.65 (0.23)	2.76 (0.29)	2.91 (0.22)									
K ₂ O	3.35 (0.15)	3.06 (0.08)	3.12 (0.07)	3.01 (0.09)	2.95 (0.15)	3.29 (0.33)	3.36 (0.27)	3.24 (0.31)	2.64 (0.19)	2.94 (0.26)	2.8 (0.14)									
Cl	0.11 (0.05)	0.00	0.1 (0.04)	0.11 (0.06)	0.12 (0.07)	0.00	0.13 (0.09)	0.10 (0.04)	0.16 (0.05)	0.12 (0.04)	0.11 (0.06)									
Total	98.86 (0.41)	94.15 (0.38)	94.07 (0.37)	94.59 (0.44)	94.86 (0.45)	95.45	95.51 (1.07)	95.54 (0.93)	91.88 (0.63)	94.20 (0.68)	94.42 (0.66)									
<i>n</i>	22	8	9	8	10	10	11	8	10	9	9									
Sample T (°C) Pressure (MPa)	KZI-11 ^m		KZI-12 ^c		KZI-13 ^m		KZI-14 ^c		KZI-15 ^m		KZI-16 ^c		KZI-17 ^m		KZI-18 ^c		KZI-19 ^m		KZI-20 ^c	
	850 200	200	850 200	875 200	875 200	875 200	875 200	825 250	825 250	825 250	825 250	815 125	815 125	815 125	860 125	860 125	860 125	860 125	860 125	860 125
SiO ₂	68.20 (0.62)	67.92 (0.52)	66.93 (0.74)	67.19 (0.79)	67.85 (0.81)	68.16 (0.84)	71.13 (0.73)	71.04 (0.71)	73.59 (0.74)	73.64 (0.77)										
Al ₂ O ₃	14.93 (0.17)	15.14 (0.16)	15.82 (0.18)	15.66 (0.22)	15.64 (0.20)	16.18 (0.26)	13.94 (0.23)	14.12 (0.15)	11.74 (0.16)	11.92 (0.19)										
TiO ₂	0.22 (0.02)	0.19 (0.04)	0.11 (0.04)	0.12 (0.05)	0.28 (0.05)	0.26 (0.07)	0.21 (0.07)	0.22 (0.09)	0.31 (0.08)	0.28 (0.11)										
FeO _{tot}	1.58 (0.09)	1.61 (0.11)	1.72 (0.44)	1.78 (0.32)	1.75 (0.41)	1.64 (0.43)	1.98 (0.09)	1.96 (0.16)	1.18 (0.14)	1.20 (0.13)										
MgO	0.22 (0.04)	0.24 (0.08)	0.26 (0.06)	0.25 (0.06)	0.26 (0.14)	0.22 (0.09)	0.21 (0.08)	0.22 (0.05)	0.12 (0.09)	0.16 (0.04)										
CaO	0.98 (0.18)	1.08 (0.14)	1.13 (0.06)	1.18 (0.05)	1.18 (0.05)	1.11 (0.08)	0.98 (0.14)	0.96 (0.17)	0.96 (0.08)	0.92 (0.15)										
Na ₂ O	2.61 (0.11)	2.6 (0.17)	2.58 (0.34)	2.46 (0.41)	2.39 (0.48)	2.22 (0.44)	3.48 (0.24)	3.57 (0.22)	3.14 (0.28)	3.11 (0.12)										
K ₂ O	2.61 (0.20)	2.62 (0.23)	2.57 (0.25)	2.59 (0.27)	2.48 (0.28)	2.55 (0.31)	3.11 (0.17)	3.18 (0.19)	3.21 (0.14)	3.25 (0.17)										
Cl	0.10 (0.04)	0.05 (0.05)	0.11 (0.04)	0.13 (0.05)	0.14 (0.06)	0.16 (0.07)	0.11 (0.04)	0.12 (0.07)	0.10 (0.03)	0.09 (0.03)										
Total	91.45 (0.52)	91.45 (0.51)	91.23 (0.79)	91.36 (0.74)	91.97 (1.04)	92.50 (0.98)	95.15 (0.81)	95.39 (0.75)	94.35 (0.79)	94.57 (0.77)										
<i>n</i>	10	9	8	9	6	10	11	9	9	10										

n, number of analyses averaged; (), analytical standard deviation; ^m, melting experiments; ^c, crystallization experiments.

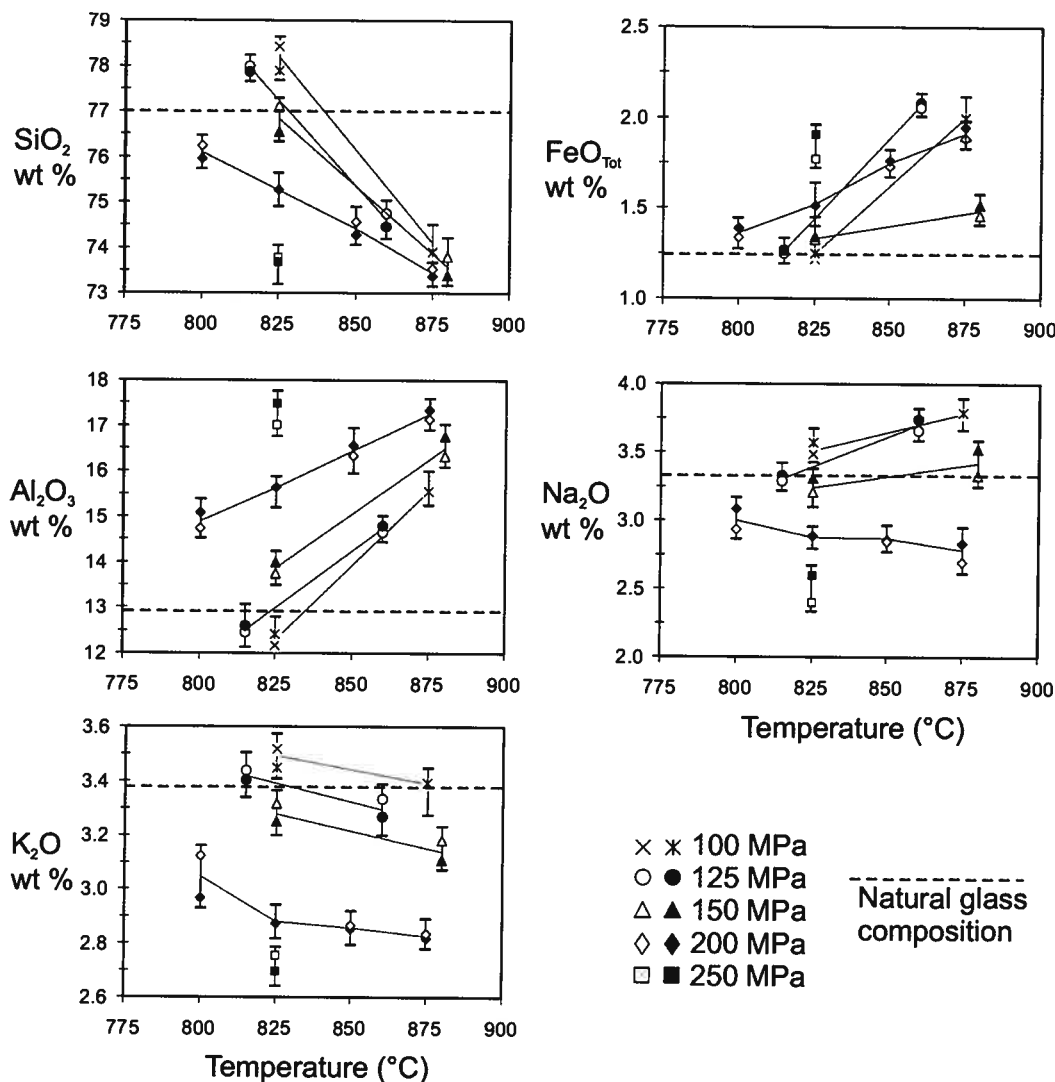


Figure 4. Normalized matrix glass compositions from natural KZI dacite (dashed line) and hydrothermal experiments for different pressures and temperatures (Table 5). Solid lines connect experiments conducted at equal pressures. Melting and crystallization experiments (open and solid symbols, respectively) used both pre-run aliquots and 01BBKZ-1 crushed KZI dacite pumice (Table 3).

even though in some experiments the concentration of S included was only 0.1 wt%. In contrast, phase equilibria experiments saturated with H₂O alone did not result in the crystallization of biotite or pyrrhotite (Costa *et al.* 2004). Because no such discrepancy in mineral assemblage is observed between experimentally derived KZI dacite samples and the natural KZI dacite starting material in this study; however, we are confident that our results accurately depict the pre-eruptive storage conditions in terms of temperature, pressure and fO_2 .

The inferred pre-eruptive storage conditions of 5–6 km depth for the KZI dacite corresponds to the location of a structural discontinuity between upper Miocene volcanoclastic sedimentary rocks of the Shchapinsky suite and late Pliocene–Pleistocene-aged volcanic rocks that underlie Kizimen Volcano (Shantser *et al.* 1976). Indeed, the

presence of structural discontinuities, which are particularly susceptible to processes such as fracturing and slip in response to changes in the regional stress field, may facilitate physical conditions favourable for the transport and accumulation of magma (e.g. Frazzetta and Villari 1981; Hoshizumi *et al.* 1999; Vigneresse and Clemens 2000; Márquez *et al.* 2001). However, although structural discontinuities in the upper crust may enhance magma transport and emplacement to some degree, their role in the long-term storage of magma over the lifetime of a volcano is uncertain as evidenced by studies that experimentally constrain the pre-eruptive storage conditions of magmas erupted over these time periods. For example, Gardner *et al.* (1995) found that magma storage conditions varied significantly over the past 4000 years at Mount St Helens (USA), where magma emplacement depths varied from 6 to 12 km despite the existence of a structural discontinuity located approximately 16 km below Mount St Helens (Lees 1992). Results from Gardner *et al.* (1995) indicate that the 'Bi' and 'Wn' eruptive units, which are separated by ~1200 years, tapped magma from a 6 km storage depth followed by a 12 km depth. Then, two years later, magma stored at 7.5 km depth was erupted as the 'We' unit of the Kalama eruptive period (Gardner *et al.* 1995). In contrast, Scaillet *et al.* (2008) found that the pre-eruptive storage depths of magma erupted from Mount Vesuvius (Italy) has steadily decreased from 11–12 to 3–4 km over the past 20,000 years despite the inferred presence of a prominent structural discontinuity located approximately 11–15 km beneath the Vesuvius edifice (De Natale *et al.* 2006).

Whereas upper crustal structural discontinuities appear unable to serve effectively as magma storage reservoirs over the long term (i.e. $\sim 10^3$ – 10^4 years), experimental evidence presented here indicate that the KZI dacite last crystallized at a depth that corresponds to a 5–6 km-deep structural discontinuity prior to eruption. How long did this magma reside at this depth prior to eruption? Many recent studies utilizing high-resolution compositional analysis of mineral phases to model crystal-melt diffusion timescales coupled with geochronology methods from small volume eruptions of intermediate magmas suggest that timescales of magma storage prior to eruption may range from <10 to $<10^3$ years (e.g. Turner *et al.* 2000; Zellmer *et al.* 2003; Costa and Dungan 2005; Jicha *et al.* 2006). Certainly, a short-lived pre-eruptive storage period at 5–6 km depth agrees with Sr and Nd isotopic results from basalt, basaltic andesite, and dacite samples erupted during Kizimen's KZI and KZIV eruptive periods, which show no evidence for assimilation of surrounding country rock (Churikova *et al.* 2007). A short-lived storage scenario at the pressures and temperatures determined in this study also supports the finding that many dacite samples erupted during the KZI eruptive period are characterized by abundant quenched basaltic enclaves and a complex disequilibria mineral assemblage of plagioclase, hornblende, orthopyroxene, clinopyroxene, olivine, titanomagnetite, and ilmenite, which formed as a result of incomplete mixing between a basaltic and dacitic magma shortly before eruption (Churikova *et al.* 2001a; 2007).

We are confident that further study of the Kizimen volcano magma plumbing system will contribute a great deal to our understanding of magma accumulation and storage, which will ultimately increase our ability to interpret petrological and experimental data more effectively.

Acknowledgements

We are deeply appreciative to be involved in research in such a dynamic and fascinating region and are especially grateful to Boris Ivanov, Oxana Evdokimova, Evgeni Gordeev, Alexander Belousov,

James Gardner, Jessica Larsen, Diane Clemens-Knott, and Gary Ernst for their scientific insight and friendship. We also thank Frank Kyte and Ken Severin for assistance with the UCLA JEOL Superprobe and UAF Cameca SX-50 microprobe, respectively; and the Cal State Fullerton Office of Grants and Contracts for financial support of this research. Finally, we thank our families for their enthusiasm and patience.

References

- Anderson, D.J., and Lindsley, D.H., 1988, Internally consistent solution models for Fe–Mg–Mn–Ti Oxides: Fe–Ti oxides: *American Mineralogist*, v. 73, p. 714–726.
- Bacon, C.R., and Hirschmann, M.M., 1988, Mg/Mn partitioning as a test for equilibrium between coexisting Fe–Ti oxides: *American Mineralogist*, v. 73, p. 57–61.
- Barclay, J., Rutherford, M.J., Carroll, M.R., Murphy, M.D., Devine, J.D., Gardner, J., and Sparks, R.S.J., 1998, Experimental phase equilibria constraints on pre-eruptive storage conditions of the soufriere hills magma: *Geophysical Research Letters*, v. 25, p. 3437–3440.
- Browne, B., and Gardner, J., 2006, The influence of magma ascent path on the texture, mineralogy, and formation of hornblende reaction rims: *Earth and Planetary Science Letters*, v. 246, p. 161–176.
- Carroll, M.R., and Webster, J.D., 1994, Solubilities of sulfur, noble gases, nitrogen, chlorine, and fluorine in magmas: *Reviews in Mineralogy and Geochemistry*, v. 30, p. 231–279.
- Churikova, T.G., Dorendorf, F., and Wörner, G., 2001a, Sources and fluids in the mantle wedge below Kamchatka, evidence from across-arc geochemical variation: *Journal of Petrology*, v. 42, p. 1567–1593.
- Churikova, T.G., Ivanov, B., Eichelberger, J., Trusov, S., Gardner, J., Belousov, A., Browne, B., Izbekov, P., and Wörner, G., 2001b, Kizimen volcano: an unzen-like magma system in Kamchatka [abstract]: *Eos Transactions of the American Geophysical Union*, v. 82, V42D–1062.
- Churikova, T.G., Wörner, G., Eichelberger, J., and Ivanov, B., 2007, Minor- and trace element zoning in plagioclase from Kizimen volcano, Kamchatka: Insights on the magma chamber processes: *American Geophysical Union Monograph Series*, v. 172, p. 303–323.
- Costa, F., Scaillet, B., and Pichavant, M., 2004, Petrological and experimental constraints on the pre-eruption conditions of holocene dacite from Volcán San Pedro (36°S, Chilean Andes) and the importance of sulphur in silicic subduction-related magmas: *Journal of Petrology*, v. 45, p. 855–881.
- Costa, F., and Dungan, M., 2005, Short time scales of magmatic assimilation from diffusion modeling of multiple elements in olivine: *Geology*, v. 33, p. 837–840.
- De Natale, G., Troise, C., Pingue, F., Mastrolorenzo, G., and Pappalardo, L., 2006, The Somma–Vesuvius volcano (Southern Italy): Structure, dynamics and hazard evaluation: *Earth-Science Reviews*, v. 74, p. 73–111.
- Devine, J.D., Gardner, J.E., Brack, H.P., Layne, G.D., and Rutherford, M.J., 1995, Comparison of microanalytical methods for estimating H₂O contents of silicic volcanic glasses: *American Mineralogist*, v. 80, p. 319–328.
- Frazzetta, G., and Villari, L., 1981, The feeding of the eruptive activity of Etna Volcano. The regional stress field as a constraint to magma uprising: *Journal of volcanology and Geothermal Research*, v. 112, p. 175–187.
- Gardner, J.E., Rutherford, M., Carey, S., and Sigurdsson, H., 1995, Experimental constraints on pre-eruptive water contents and changing magma storage prior to explosive eruptions of Mount St Helens Volcano: *Bulletin of Volcanology*, v. 57, p. 1–17.
- Geschwind, C., and Rutherford, M.J., 1992, Cummingtonite and the evolution of the Mount St. Helens (Washington) magma system; An experimental study: *Geology*, v. 20, p. 1011–1014.
- Grove, T.L., Donnelly-Nolan, J.M., and Housh, T.B., 1997, Magmatic processes that generated the rhyolite of Glass Mountain, Medicine Lake Volcano, N. California: *Contributions to Mineralogy and Petrology*, v. 127, p. 205–223.
- Hammer, J.E., and Rutherford, M.J., 2002, An experimental study of the kinetics of decompression-induced crystallization in silicic melt: *Journal of Geophysical Research*, v. 107, p. 1–24.
- Hoshizumi, H., Uto, K., and Watanabe, K., 1999, Geology and eruptive history of Unzen volcano, Shimabara Peninsula, Kyushu, SW Japan: *Journal of Volcanology and Geothermal Research*, v. 89, p. 81–94.

- Izbekov, P., Gardner, J.E., and Eichelberger, J.C., 2004, Comagmatic granophyre and dacite from Karymsky volcanic center, Kamchatka: Experimental constraints for magma storage conditions: *Journal of Volcanology and Geothermal Research*, v. 131, p. 1–18.
- Jicha, B.R., Scholl, D.W., Singer, B.S., Yogodzinski, G.M., Kay, S.M., 2006, Revised age of Aleutian Island Arc Formation implies high rate of magma production: *Geology*, v. 34, p. 661–664.
- Larsen, J.F., and Gardner, J.E., 2000, Experimental constraints on bubble interactions in rhyolitic melts: Implications for vesicle size distributions: *Earth and Planetary Science Letters*, v. 180, p. 201–214.
- Lees, J.M., 1992, The magma system of Mount St. Helens: non-linear high-resolution P-wave tomography: *Journal of Volcanology and Geothermal Research*, v. 53, p. 103–116.
- Márquez, A., Oyarzun, R., de Ignacio, C., and Doblas, M., 2001, Soutward migration of volcanic activity in the central Mexican Volcanic Belt: asymmetric extension within a two-layer crustal stretching model: *Journal of Volcanology and Geothermal Research*, v. 112, p. 175–187.
- Melekestsev, I.V., Ponomareva, V.V., and Volynets, O.N., 1995, Kizimen Volcano, Kamchatka – A Future Mount St. Helens?: *Journal of Volcanology and Geothermal Research*, v. 65, p. 205–226.
- Piip, B.I., 1946, Kizimen volcano: *Bulletin of Volcanology Stantsii*, v. 13, p. 22–32 (in Russian).
- Rutherford, M.J., and Devine, J.D., 1996, Pre-eruption pressure-temperature conditions and volatiles in the 1991 Mount Pinatubo magma, *in* Newhall, C.G., and Punongbayan, R.S., eds., *Fire and mud, eruptions and lahars of Mount Pinatubo, Philippines*: Seattle, University of Washington Press, p. 751–766.
- Rutherford, M.J., Sigurdsson, H., Carey, S., and Davis, A., 1985, The May 18, 1980, Eruption of Mount St. Helens; 1, melt composition and experimental phase equilibria: *Journal of Geophysical Research*, v. 90, p. 2929–2947.
- Sato, H., Nakada, S., Fujii, T., Nakamura, M., and Suzuki-Kamata, K., 1999, Groundmassargasite in the 1991–1995 dacite of Unzen volcano: Phase stability experiments and volcanological implications: *Journal of Volcanology and Geothermal Research*, v. 89, p. 197–212.
- Scaillet, B., and Evans, W.E., 1999, The 15 June 1991 eruption of Mount Pinatubo. I. Phase equilibria and pre-eruption P–T– f_{O_2} – f_{H_2O} conditions of the dacite magma: *Journal of Petrology*, v. 40, p. 381–411.
- Scaillet, B., and Pichavant, M., 2003, Experimental constraints on volatile abundances in arc magmas and their implications for degassing processes, *in* Oppenheimer, C., Pyle, D., and Barclay, J., eds., *Volcanic degassing*: London, Geological Society, Special Publications, vol. 213, p. 23–52.
- Scaillet, B., Pichavant, M., and Cioni, R., 2008, Upward migration of Vesuvius magma chamber over the past 20,000 years: *Nature*, v. 455, p. 216–219.
- Shantser, A.E., Kutuyev, F.Sh., and Pertov, V.S., 1976, Kizimen volcano. *Bulletin Volcanology Stantsii*, v. 49, p. 24–29 (in Russian).
- Stormer, J.C., 1983, The effects of recalculation on estimates of temperature and oxygen fugacity from analyses of multi-component iron–titanium oxides: *American Mineralogist*, v. 68, p. 586–594.
- Turner, S.P., George, R.M.M., Evans, P.J., Hawkesworth, C.J., and Zellmer, G.F., 2000, Timescales of magma formation, ascent and storage beneath subduction-zone volcanoes: *Philosophical transactions: Mathematical, Physical and Engineering Sciences*, v. 358, p. 1443–1464.
- Vignerresse, J.L., and Clemens, J.D., 2000, Granitic magma ascent and emplacement: neither diapirism nor natural buoyancy: *Geological Society, London, Special Publications*, v. 174, p. 1–19.
- Wallace, P., 2005, Volatiles in subduction zone magmas: concentrations and fluxes based on melt inclusion and volcanic gas data: *Journal of Volcanology and Geothermal Research*, v. 140, p. 217–240.
- Zellmer, G.F., Sparks, R.S.J., Hawkesworth, C.J., and Wiedenbeck, M., 2003, Magma emplacement and remobilization timescales beneath Montserrat: Insights from Sr and Ba zonation in plagioclase phenocrysts. *Journal of Petrology*, v. 44, p. 1413–1431.